Title

Magnetite Biomineralization in Magnetospirillum magneticum Is Regulated by a Switch-like Behavior in the HtrA Protease MamE*

Journal

Journal of Biological Chemistry, 291(34)

ISSN

0021-9258

Authors

Hershey, David M
Browne, Patrick J
Iavarone, Anthony T
et al.

Publication Date

2016-08-01

DOI

10.1074/jbc.m116.731000

THE JOURNAL OF BIOLOGICAL CHEMISTRY VOL. 291, NO. 34, pp. 17941–17952, August 19, 2016

Magnetite Biomineralization in *Magnetospirillum magneticum* Is Regulated by a Switch-like Behavior in the HtrA Protease MamE*

Received for publication, April 4, 2016, and in revised form, June 8, 2016 Published, JBC Papers in Press, June 14, 2016, DOI 10.1074/jbc.M116.731000

David M. Hershey[‡], Patrick J. Browne[‡], Anthony T. Iavarone[§¶], Joan Teyra[‖], Eun H. Lee[**], Sachdev S. Sidhu[‖], and Arash Komeili[‡§1]**

*From the Departments of [‡]Plant and Microbial Biology and [**]Molecular and Cell Biology, the [§]*California Institute for Quantitative Biosciences, and the *[¶]QB3/Chemistry Mass Spectrometry Facility, and the University of California, Berkeley, California 94720 and the [‖]Department of Molecular Genetics, Terrance Donnelly Centre for Cellular and Biomedical Research, University of Toronto, Toronto, Ontario M5S 3E1, Canada*

Magnetotactic bacteria are aquatic organisms that produce subcellular magnetic particles in order to orient in the earth's geomagnetic field. MamE, a predicted HtrA protease required to produce magnetite crystals in the magnetotactic bacterium *Magnetospirillum magneticum* AMB-1, was recently shown to promote the proteolytic processing of itself and two other biomineralization factors *in vivo*. Here, we have analyzed the *in vivo* processing patterns of three proteolytic targets and used this information to reconstitute proteolysis with a purified form of MamE. MamE cleaves a custom peptide substrate with positive cooperativity, and its autoproteolysis can be stimulated with exogenous substrates or peptides that bind to either of its PDZ domains. A misregulated form of the protease that circumvents specific genetic requirements for proteolysis causes biomineralization defects, showing that proper regulation of its activity is required during magnetite biosynthesis *in vivo*. Our results represent the first reconstitution of the proteolytic activity of MamE and show that its behavior is consistent with the previously proposed checkpoint model for biomineralization.

Magnetotactic bacteria assemble iron-based magnetic crystals called magnetosomes into chains within their cells, allowing them to passively align in and navigate along magnetic fields (1, 2). Understanding the mechanism of biomineralization in these organisms can provide novel strategies for manipulating transition metal-based nanomaterials *in vitro* (3–5). Genetic analyses have identified a set of genes, called biomineralization factors, whose deletions disrupt or eliminate magnetite crystal formation (6–10). Two of these, *mamE* and *mamO*, encode predicted trypsin-like proteases required to produce magnetite in the model magnetotactic organism, *Magnetospirillum magneticum* AMB-1 (6). Disrupting either gene abolishes the formation of magnetite crystals without disturbing the production of their surrounding membrane compartment, showing that each protein is required for initiating magnetite biosynthesis (6, 11, 12).

Cells with a catalytically inactive (E^{PD}) allele of *mamE* show an intermediate biomineralization phenotype in which they produce small magnetite particles. Wild-type AMB-1 has a distribution of crystal sizes centered at 50–60 nm in diameter, but the size distribution in the E^{PD} cells is centered at ~20 nm. Interestingly, ~97% of the crystals in the E^{PD} strain are smaller than 35 nm, the point above which magnetite particles become paramagnetic and can hold a stable magnetic dipole. The correlation between mineral sizes in the E^{PD} strain and the superparamagnetic to paramagnetic transition point lead to a model predicting that cells produce small superparamagnetic crystals until an unknown signal activates MamE, promoting maturation to paramagnetic particles (13).

MamE is a member of the HtrA/DegP family of trypsin-like proteases, a ubiquitous family of enzymes that controls various aspects of protein quality control (14). The family is characterized by domain structures consisting of an N-terminal trypsin-like domain and one or two C-terminal PDZ (postsynaptic density 95/discs large/zonula occludens-1) domains (15–17). Structural and mechanistic investigations indicate that the PDZ domains regulate proteolysis by promoting assembly and activating the protease domain by binding to extended peptide motifs (18–23). Recently, MamE was found to promote the *in vivo* proteolytic processing of itself, MamO, and another biomineralization factor named MamP, in a manner that required the predicted MamE active site (Fig. 1*A*) (24–26). Although MamO was also required for these proteolytic events, this effect did not require its predicted protease active site. Subsequent structural analysis showed that the protease domain of MamO was locked in an inactive state and incapable of catalysis, suggesting that it played a non-catalytic role in activating MamE (24).

Despite the genetic evidence for the role of MamE in proteolysis, its activity has not been confirmed directly using purified components. Studies aimed at understanding the catalytic activity of MamE and its regulation have been hindered by an inability to obtain recombinant protein. Here, we have characterized MamE-dependent proteolysis in detail and identified a number of regulatory mechanisms. Developing a method to

* This work was supported by National Institutes of Health Grant R01GM084122, National Science Foundation Grant 1504610, and Office of Naval Research Grant N000141310421 (to A. K.). The authors declare that they have no conflicts of interest with the contents of this article. The content is solely the responsibility of the authors and does not necessarily represent the official views of the National Institutes of Health.

[1] To whom correspondence should be addressed: Dept. of Plant and Microbial Biology, University of California, 261 Koshland Hall, Berkeley, CA 94720. E-mail: komeili@berkeley.edu.

TABLE 1
Strains used in this study

Strain	Organism	Description	Source/Reference
AK30	*M. magneticum* AMB-1	Wild-type AMB-1	Ref. 6
AK69	*M. magneticum* AMB-1	Δ*mamP*	Ref. 6
AK96	*M. magneticum* AMB-1	Δ*mamE* Δ*limE*	Ref. 13
AK94	*M. magneticum* AMB-1	Δ*mamO* Δ*R9*	Ref. 13
AK205	*M. magneticum* AMB-1	Δ*mamE* Δ*mamO* Δ*R9*	Ref. 24
C43	*E. coli*	Protein expression strain	Lucigen
BL21 CodonPlus	*E. coli*	Protein expression strain; Cm^R	Agilent
DH5α (λ*pir*)	*E. coli*	Standard cloning strain	Ref. 6
WM3064	*E. coli*	Mating strain; DAP auxotroph used for plasmid transfer	Ref. 6

TABLE 2
Plasmids used in this study

Plasmid	Description	Source/Reference
pAK605	Plasmid for expressing protein under control of the *mamH* promoter; non-replicative in AMB-1: integrates upstream of amb0397	Ref. 24
pAK701	pAK605 containing N-terminally 3× FLAG-tagged *mamE*	This work
pAK702	pAK605 containing C-terminally 3× FLAG-tagged *mamE*	This work
pAK787	pAK605 containing N-terminally 3× FLAG-tagged *mamP*	This work
pAK788	pAK605 containing C-terminally 3× FLAG-tagged *mamP*	This work
pAK823	pAK605 containing N-terminally 3× FLAG-tagged *mamO*	Ref. 24
pAK1003	pAK605 containing C-terminally 3× FLAG-tagged *mamO*	This work
pAK1005	pLBM4; LIC compatible vector for expressing fusions to the OmpA signal peptide under the control of the *lac* promoter	Ref. 28
pAK1004	pEC86; plasmid constitutively expressing the *E. coli ccm* genes for *c*-type cytochrome maturation	Ref. 29
pAK825	pLBM4 containing His_6-TEV-MamE(108–728)-strep fused to the OmpA signal peptide	This work
pAK964	pAK825 with the S297A mutation in MamE	This work
pAK619	pAK605 containing *mamE*	Ref. 24
pAK620	pAK605 containing $mamE^{PD}$ (H188A/T211A/S297A mutant)	Ref. 24
pAK999	pAK605 containing $mamE^{QP}$ (Q294P mutant)	This work
pAK1000	pET-based vector expressing the first PDZ domain of MamE(489–588) fused to His_6-MBP-TEV at the N terminus	This work
pAK1001	pET-based vector expressing the second PDZ domain of MamE(634–728) fused to His_6-MBP-TEV at the N terminus	This work
pAK1002	pET-based vector expressing the first and second PDZ domains of MamE(489–728) fused to His_6-MBP-TEV at the N terminus	This work

purify MamE and analyzing *in vivo* proteolytic patterns of each target facilitated reconstitution of MamE-dependent proteolysis *in vitro*. Detailed analysis of its catalytic activity suggests a switch-like model in which the basal state of the protein is an inactive form that can be turned on through a number of routes. A constitutively active allele of MamE disrupts biomineralization, confirming that properly regulated proteolysis is critical to magnetosome formation.

Experimental Procedures

Strains, Plasmids, and Growth Conditions—The strains and plasmids used in this study are described in Tables 1 and 2, respectively. AMB-1 was maintained in MG medium supplemented with kanamycin when necessary, as described previously (6). Magnetic response was measured using the coefficient of magnetism as described previously (6). Standard molecular biology techniques were used for plasmid manipulation. *Escherichia coli* strains were grown in LB medium supplemented with appropriate antibiotics. Plasmids were maintained in *E. coli* strain DH5α λ*pir*. *E. coli* strain WM3064 was used for plasmid conjugations as described previously (6).

Immunoblotting—Whole-cell lysates of AMB-1 strains were prepared from 10-ml cultures and analyzed as described previously (24). For analysis of the autocleavage reaction products, a 1:10 dilution of each time point was separated on a 12% (v/v) acrylamide gel for immunoblotting. The MamE and MamP antibodies have been described previously (24). The anti-His_6 (Sigma), anti-FLAG (Sigma), anti-σ70 (Thermo Fisher), and anti-Strep-tag (Qiagen) antibodies were purchased from commercial sources.

Fractionation of MamO Fragments—A strain with the genetic background Δ*O*Δ*R9*/*FLAG-O* was cultured without shaking at 30 °C in 2-liter screw-capped flasks that were filled to the top with MG medium. The cells were harvested by centrifuging at 5,000 × *g* for 15 min; resuspending in 20 ml of cold 25 mM Tris-HCl, pH 7.4; recentrifuging at 8,000 × *g* for 10 min; and freezing the resulting pellet at −80 °C until use. Cell pellets were thawed on ice and resuspended in 5 ml of lysis buffer A (10 mM Tris-HCl, pH 8.0, 50 mM NaCl, 1 mM EDTA). Pepstatin A and leupeptin were added to a final concentration of 2 μg/ml, and PMSF was added to 2 mM. Lysozyme was added from 50 mg/ml stock to a final concentration of 0.5 mg/ml, and the cells were incubated at room temperature for 15 min. 15 ml of lysis buffer B (20 mM HEPES-KOH, pH 7.5, 50 mM NaCl, 1.25 mM $CaCl_2$) was added along with DTT to 2 mM and DNase to 5 μg/ml, and the suspension was incubated for 15 min at 4 °C with agitation. The cells were sonicated twice for 10 s, and the suspension was centrifuged at 8,000 × g for 10 min to isolate the magnetite-associated material.

The resulting pellet was resuspended in 5.5 ml of solubilization buffer (20 mM BisTris[2]-HCl, pH 7.0, 75 mM NaCl, 10% (v/v) glycerol), and CHAPS was added to 1% (w/v) from a 10% (w/v) stock solution. The suspension was incubated at room temperature for 15min with agitation followed by an incubation for 15 min at 4 °C with agitation. The suspension was centrifuged at 16,000 × *g* for 15 min. The resulting pellet was resuspended in 5.5 ml of solubilization buffer, and the detergent extraction was repeated with 1% (w/v) FosCholine. The FosCholine-soluble material was loaded on a 1-ml HiTrap Q FF column (GE Healthcare) that had been equilibrated with solubilization

[2] The abbreviations used are: BisTris, 2-[bis(2-hydroxyethyl)amino]-2-(hydroxymethyl)propane-1,3-diol; DDM, *n*-dodecyl β-D-maltoside; Ni-NTA, nickel-nitrilotriacetic acid; TEV, tobacco etch virus; MBP, maltose-binding protein.

buffer containing 0.03% (w/v) *n*-dodecyl β-D-maltoside (DDM). The column was washed with 10 ml of solubilization buffer with 0.03% (w/v) DDM and eluted with 4 ml of buffer Q1 (20 mM BisTris-HCl, pH 7.0, 275 mM NaCl, 10% (v/v) glycerol) with 0.03% (w/v) DDM followed by 4 ml of buffer Q2 (20 mM BisTris-HCl, pH 7.0, 400 mM NaCl, 10% (v/v) glycerol) with 0.03% (w/v) DDM. The Q1 fraction was added to 50 μl of anti-FLAG M2 resin (Sigma) and incubated at 4 °C with agitation for 3 h. The resin was isolated by centrifuging at 4,000 × *g* and washed with sequential 1-ml washes of buffer Q2, buffer Q1, and solubilization buffer, each containing 0.03% (w/v) DDM. Bound proteins were eluted by three washes with 50 μl of 0.2 M glycine, pH 2.8, which were then pooled with 50 μl of 1 M Tris-HCl, pH 8.0.

Preparation of Trypsin Digests for LC-MS—The concentrated FLAG elution fraction was separated on a 12% (w/v) acrylamide gel and stained with colloidal Coomassie Blue. A ~3 × 10-mm section of the gel corresponding to the processed MamO band was excised from the gel and chopped into small pieces. These were washed with 100 mM NH_4HCO_3 followed by reduction and alkylation of cysteines with DTT and iodoacetamide. The gel pieces were then dehydrated by washing with increasing concentrations of acetonitrile in 100 mM NH_4HCO_3 and dried under vacuum. A 0.1 mg/ml solution of trypsin was used to re-swell the gel pieces, and they were incubated overnight at 37 °C. The resulting peptides were extracted from the gel slices with successive washes of 0.1% (v/v) formic acid solutions containing increasing concentrations of acetonitrile. The extracts were pooled in a fresh tube, concentrated under vacuum to remove the organic phase, and stored at 4 °C until analysis.

LC-MS—Trypsin-digested protein samples were analyzed using a Thermo Dionex UltiMate3000 RSLCnano liquid chromatograph that was connected in-line with an LTQ-Orbitrap-XL mass spectrometer equipped with a nanoelectrospray ionization source (Thermo Fisher Scientific, Waltham, MA). The LC was equipped with a C18 analytical column (Acclaim® PepMap RSLC, 150-mm length × 0.075-mm inner diameter, 2-μm particles, 100-Å pores; Thermo) and a 1-μl sample loop. Acetonitrile (Fisher Optima grade, 99.9% (v/v)), formic acid (1-ml ampules, 99+% (v/v), Thermo Pierce), and water purified to a resistivity of 18.2 megaohms·cm (at 25 °C) using a Milli-Q Gradient ultrapure water purification system (Millipore, Billerica, MA) were used to prepare mobile phase solvents. Solvent A was 99.9% water, 0.1% (v/v) formic acid, and solvent B was 99.9% acetonitrile, 0.1% (v/v) formic acid. The elution program consisted of isocratic flow at 2% B for 4 min, a linear gradient to 30% B over 38 min, isocratic flow at 95% B for 6 min, and isocratic flow at 2% B for 12 min at a flow rate of 300 nl/min.

Full-scan mass spectra were acquired in the positive ion mode over the range $m/z = 350–1{,}800$ using the Orbitrap mass analyzer, in profile format, with a mass resolution setting of 60,000 (at $m/z = 400$, measured at full width at half-maximum peak height), which provided isotopic resolution for singly and multiply charged peptide ions. Thus, an ion's mass and charge could be determined independently (*i.e.* the charge state was determined from the reciprocal of the spacing between adjacent isotope peaks in the m/z spectrum). In the data-dependent mode, the eight most intense ions exceeding an intensity threshold of 50,000 counts were selected from each full-scan mass spectrum for tandem mass spectrometry (MS/MS) analysis using collision-induced dissociation. MS/MS spectra were acquired using the linear ion trap, in centroid format, with the following parameters: isolation width, 3 m/z units; normalized collision energy, 30%; default charge state, 3+; activation Q, 0.25; and activation time, 30 ms. Real-time charge state screening was enabled to exclude unassigned and 1+ charge states from MS/MS analysis. Real-time dynamic exclusion was enabled to preclude reselection of previously analyzed precursor ions, with the following parameters: repeat count 2, repeat duration 10 s, exclusion list size 500, exclusion duration 90 s, and exclusion mass width 20 ppm. Data acquisition was controlled using Xcalibur software (version 2.0.7, Thermo). Raw data were searched against the *M. magneticum* AMB-1 FASTA protein database using Proteome Discoverer software (version 1.3, SEQUEST algorithm, Thermo). Peptide identifications were validated by manual inspection of MS/MS spectra (*i.e.* to check for the presence of y-type and b-type fragment ions that identify the peptide sequences) (27).

Expression and Purification of MamE—In the expression construct used to purify MamE, the N-terminal membrane anchor is replaced with the OmpA signal peptide to produce a soluble protein that can still undergo heme loading in the periplasm (28). Initial fractionations with an N-terminally His_6-tagged form of the protein had significant contamination due to what appeared to be truncated fragments caused by autocleavage during expression. To eliminate this problem, a Strep-tag was added on the C terminus to allow for a sequential affinity isolation of full-length protein. Finally, MamE has a predicted region of 60–70 disordered residues downstream of the N-terminal membrane anchor and upstream of the trypsin-like domain. Removing this region dramatically improved the solubility.

The plasmids pAK825 or pAK964 were transferred to C43 cells (Lucigen) that had been previously transformed with the pEC86 heme-loading plasmid (29). The transformed cells were maintained at 30 °C due to growth defects caused by the plasmids at 37 °C. An overnight liquid culture was inoculated into 600 ml of 2× YT medium supplemented with the appropriate antibiotics. The cultures were grown at 30 °C until the A_{600} reached ~0.5, at which point the culture was transferred to 20 °C. After a 30-min equilibration, the culture was induced with 35 μM isopropyl 1-thio-β-D-galactopyranoside. Expression was performed for 12.5–13 h at 20 °C with shaking at 200 rpm.

Cells were harvested by immediately chilling the cultures on ice and centrifuging at 6,000 × *g* for 10 min. The resulting pellet was resuspended in 50 ml of cold osmotic shock buffer (50 mM sodium phosphate, pH 8.0, 1 mM EDTA, 20% (w/v) sucrose). Leupeptin (1.5 μg/ml), pepstatin A (1.5 μg/ml), and lysozyme (0.5 mg/ml) were added, and the suspension was rocked at room temperature for 15 min. An equal volume of ice-cold H_2O was added, and the suspension was rocked on ice for 15 min before centrifuging at 8,000 × *g* for 10 min to remove debris.

The resulting supernatant was added to 3 ml of Ni-NTA resin (Qiagen) and supplemented with NaCl (150 mM), DNase I (5

μg/ml), Nonidet P-40 (0.1% (v/v)), and $MgCl_2$ (2.5 mM). The slurry was rocked at 4 °C for 30 min, and the beads were allowed to settle. After decanting the upper phase, the slurry was poured into a column, washed with 10 column volumes of nickel wash buffer (25 mM Tris-HCl, pH 7.4, 250 mM NaCl, 10 mM imidazole, 10% (v/v) glycerol), and the bound proteins were eluted with nickel elution buffer (25 mM Tris-HCl, pH 7.4, 250 mM NaCl, 250 mM imidazole, 10% (v/v) glycerol). The Ni-NTA eluent was loaded onto a 1-ml StrepTrap column (GE Healthcare), which was then washed with 5 ml of Strep-tag wash buffer (25 mM Tris-HCl, pH 7.4, 250 mM NaCl, 10% (v/v) glycerol). Bound proteins were eluted in Strep-tag wash buffer containing 2.5 mM desthiobiotin. The purified protein was concentrated in a 50-kDa cut-off ultrafilter while simultaneously removing the desthiobiotin by repeated dilution and concentration with Strep-tag wash buffer. The concentration was determined by the Bradford method using BSA to prepare a standard curve. Aliquots were frozen in liquid N_2 and stored at −80 °C until use.

Analysis of MamO1 Peptide Cleavage—A custom peptide with the sequence 5-carboxymethylfluorescein-Thr-Gln-Thr-Val-Ala-Ala-Gly-Ser-Lys(CPQ2)-D-Arg-D-Arg was obtained commercially (CPC Scientific). The peptide was dissolved in DMSO and stored at −20 °C. 5× substrate solutions with various concentrations of the MamO1 peptide were prepared in assay buffer (50 mM Tris-HCl, pH 8.0) containing 0.05% (v/v) Nonidet P-40 and 1.6% (v/v) DMSO. To initiate the reaction, 10-μl samples of the substrate mix were added to 40 μl of MamE protein solution that had been diluted to 125 nM in assay buffer in a 96-well plate. The fluorescence was scanned (excitation, 485 nm; emission, 538 nm) every 5 min for 2 h in a Tecan plate reader.

The slope was determined from the linear portion of each reaction. Cleavage rates were calculated by making a standard curve from a MamO1 cleavage reaction that had been incubated for 24 h to allow for complete hydrolysis. Specific activities were determined by normalizing these cleavage rates to the enzyme concentration. Rates were plotted as a function of peptide concentration and fit to the Hill form of the Michaelis-Menten equation using the Kaleidagraph software package.

$$V = \frac{V_{max}[01]^n}{K_m{}^n + [01]^n} \quad \text{(Eq. 1)}$$

Analysis of MamE Autoproteolysis—25-μl reactions were prepared by adding 1 μl of activating peptide dissolved in DMSO at the appropriate concentration to 24 μl of MamE diluted to 2 μM in assay buffer. The reactions were incubated at 30 °C, and 8-μl aliquots were removed at the appropriate times. Each aliquot was quenched immediately by mixing with SDS sample buffer. Equal volumes of each aliquot were separated on a 12% (w/v) acrylamide SDS-polyacrylamide gel and stained with Coomassie Blue to visualize the processing pattern.

Expression and Purification of PDZ Domains—For all three PDZ domain constructs (EP1, EP2, and EP12), the appropriate plasmids for expression as N-terminal His_6-MBP-TEV fusions were transformed into BL21 Codon Plus cells. Cultures were grown in 2× YT at 37 °C until the A_{600} reached ~0.8, at which point they were transferred to 20 °C for 30 min followed by induction with 0.1 mM isopropyl 1-thio-β-D-galactopyranoside and expression overnight. The cells were harvested by centrifugation, resuspended in resuspension buffer (25 mM Tris-HCl, pH 7.4, 800 mM NaCl, 10 mM imidazole, 10% (v/v) glycerol), and frozen at −80 °C until use.

For protein purification, the cells were thawed on ice and sonicated for three 30-s cycles. The lysate was clarified by centrifuging at 13,000 × *g* for 30 min. The resulting supernatant was loaded on a 3-ml Ni-NTA column that had been equilibrated in resuspension buffer. After washing with 10 column volumes of resuspension buffer and 10 column volumes of wash buffer 2 (25 mM Tris-HCl, pH 7.4, 400 mM NaCl, 25 mM imidazole, 10% (v/v) glycerol), bound proteins were eluted with nickel elution buffer.

For the purification of the EP1 and EP2 proteins, the elution fractions were dialyzed overnight against AEX buffer A (25 mM BisTris-HCl, pH 7.0, 75 mM NaCl, and 10% (v/v) glycerol). The desalted protein was passed through a 1-ml HiTrap QFF column (GE Healthcare), and the flow-through was concentrated in a 50-kDa cut-off ultrafilter, injected onto a 16/60 Superdex 200 column, and developed in storage buffer. Each protein eluted as a single symmetrical peak. The peak fractions were concentrated in a 50-kDa ultrafilter, and small aliquots were frozen in liquid N_2 and stored at −80 °C for use in the phage display experiments.

For the purification of the EP12 protein, the elution fraction was dialyzed overnight against digest buffer (50 mM sodium phosphate, pH 8.0, 75 mM NaCl, 5 mM imidazole, 10% (v/v) glycerol) in the presence of His_6-tagged TEV protease to remove the His_6-MBP tag. The resulting sample was passed through a 3-ml Ni-NTA column that had been equilibrated in digest buffer. The flow-through fraction was concentrated in a 10-kDa ultrafilter, passed through a 1-ml HiTrap SP FF column, and concentrated again before injection on a 16/60 Superdex 200 column that was developed in storage buffer. The protein eluted as a single symmetrical peak. The peak fractions were concentrated in a 10-kDa ultrafilter, and small aliquots were frozen in liquid N_2 and stored at −80 °C for use in the fluorescence anisotropy experiments.

Phage Display—C-terminally and N-terminally displayed peptide libraries were used to assess the peptide binding preferences of MamE PDZ1 and PDZ2. The C-terminal peptide library consisted of random decapeptides constructed using 10 consecutive NNK degenerate codons encoding for all 20 natural amino acids and fused to the C terminus of a mutant M13 bacteriophage major coat protein (2×10^{10} unique members) (30, 31). The N-terminal peptide library consisted of random hexadecapeptides constructed using 16 consecutive mixes of 19 codon trimers (cysteine and STOP codons were excluded) and fused to the N terminus phage coat protein (2.4×10^{11} unique members) (32).

The phage display selections followed an established protocol used previously for the PDZ human domains (33, 34). Briefly, each library was separately cycled through rounds of binding selection against each immobilized MBP-PDZ fusion protein on 96-well MaxiSorp immunoplates (Nalge Nunc). After each round, phage were propagated in *E. coli* XL1-blue

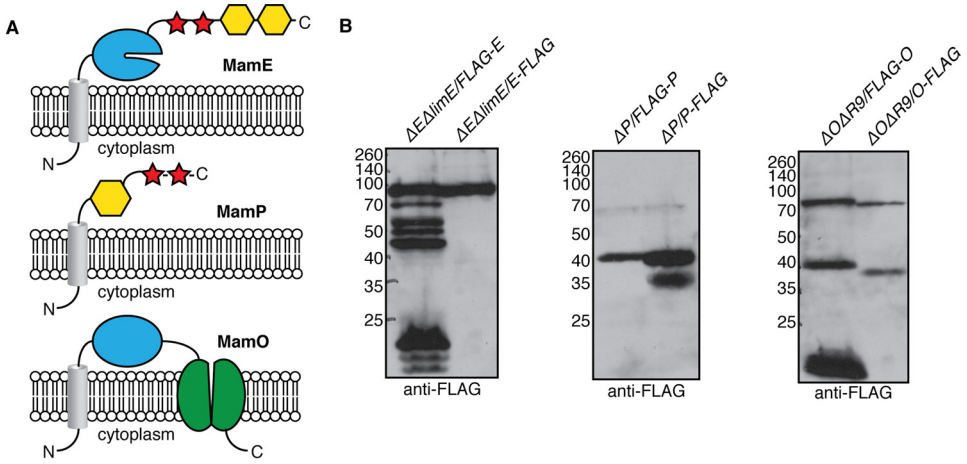

FIGURE 1. ***In vivo* proteolytic processing of MamE, MamP, and MamO.** *A*, predicted domain structures of the three proteolytic targets. *Gray cylinder*, transmembrane helix; *blue*, trypsin-like domain; *red*, *c*-type cytochrome; *yellow*, PDZ domain; *green*, TauE domain. The MamO protease domain is represented differently due to its assignment as an inactive pseudoprotease. *B*, proteolytic processing patterns observed through epitope tagging. The fragments were observed in each of at least four independent experiments with the exception of the 20-kDa N-terminal fragment of MamE and the 17-kDa N-terminal fragment of MamO, which varied dramatically between experiments.

cells (Stratagene) supplemented with M13-KO7 helper phage (New England Biolabs) to facilitate phage production. After four rounds of selection, phages from individual clones were analyzed in a phage ELISA. Phages that bound to the MBP-PDZ fusion but not a control MBP were subjected to DNA sequence analysis.

Fluorescence Anisotropy—Peptides with the following sequences were synthesized commercially with a fluorescein-aminocaproic acid group fused to the N terminus: WSQEM-EDWFWQMPLSG (PDZ1*) and MEDYGIFMTSPEGPWA (PDZ2*). Each peptide was diluted to a concentration of 40 nM in 25 mM Tris-HCl, pH 7.4, containing 0.25 mg/ml bovine serine albumin. A dilution series of EP12 protein was prepared in storage buffer. 6 μl of the ligand solution was added to 18 μl of the appropriate protein solution in a 384-well plate, and the mixture was allowed to equilibrate at room temperature for 15 min. Polarization measurements were made at 535 nm using a PerkinElmer Life Sciences Victor 3V 1420 plate reader. The resulting anisotropy values were plotted as a function of protein concentration and fit to a single site binding model using the Kaleidagraph software package.

$$FA = \frac{B_{max} \times [EP12]}{K_{D,app} + [EP12]} \qquad \text{(Eq. 2)}$$

Results

Mapping MamE-dependent Cleavage Patterns in Vivo—To determine the context of MamE-dependent proteolysis, we analyzed the cleavage patterns of MamE, MamP, and MamO using an epitope tagging approach. N- or C-terminally tagged alleles of each gene were added to their respective deletion strains. Each of the tagged alleles complemented the biomineralization defects of the deletions with the exception of the C-terminally tagged *mamO* allele (O-FLAG). For MamE, a number of N-terminal proteolytic fragments but no C-terminal fragments were observed (Fig. 1*B*), indicating that short segments are sequentially removed from the C terminus. One N-terminal and two C-terminal bands of MamP were observed, indicating the removal of a fragment containing the membrane anchor from the predicted soluble region (Fig. 1*B*). For MamO, a full-length and a shorter band were observed for both the N- and C-terminally tagged proteins, predicting an internal MamE-dependent cleavage site, resulting in two stable fragments (Fig. 1*B*). The levels and presence of the small (*i.e.* ~20 kDa) bands appearing in blots of N-terminally tagged MamE and MamO were highly inconsistent. This could suggest that short segments are removed from the N terminus of each protein to produce unstable fragments that are quickly degraded, but due to their inconsistency, we have not focused on them in our analysis of the processing pattern.

Identification of a Putative Cleavage Motif in MamO—We reasoned that one strategy for reconstituting the proteolytic activity of MamE could be to design a substrate based on an *in vivo* cleavage motif in one its targets. The MamO processing pattern indicated the presence of a ~37-kDa N-terminally tagged fragment containing a MamE-dependent cleavage site at its mature C terminus. Cell pellets from magnetic cultures of the Δ*O*Δ*R9*/*FLAG-O* strain were used for biochemical fractionation (Fig. 2*A*). Enzymatic lysis and sonication followed by a low speed (8,000 × *g*) centrifugation were used to isolate material associated with the dense magnetite particles. A number of detergents were tested for their ability to dissolve the MamO fragments. Most classes of detergents were ineffective or only partially effective in the initial solubilization step, but lipid-like zwitterionic detergents, including lauryldimethylamine oxide and FosCholine-12, efficiently extracted the fragments from the membrane. Although these detergents disrupted binding to the α-FLAG affinity resin, once the initial extraction step was complete, the detergent requirements to maintain solubility became less stringent.

Based on the solubility information, the low speed pellet was prewashed with CHAPS before extracting MamO fragments from the membranes with FosCholine-12. To facilitate binding to the affinity resin, FosCholine-soluble material was loaded on an anion exchange column and exchanged to the detergent

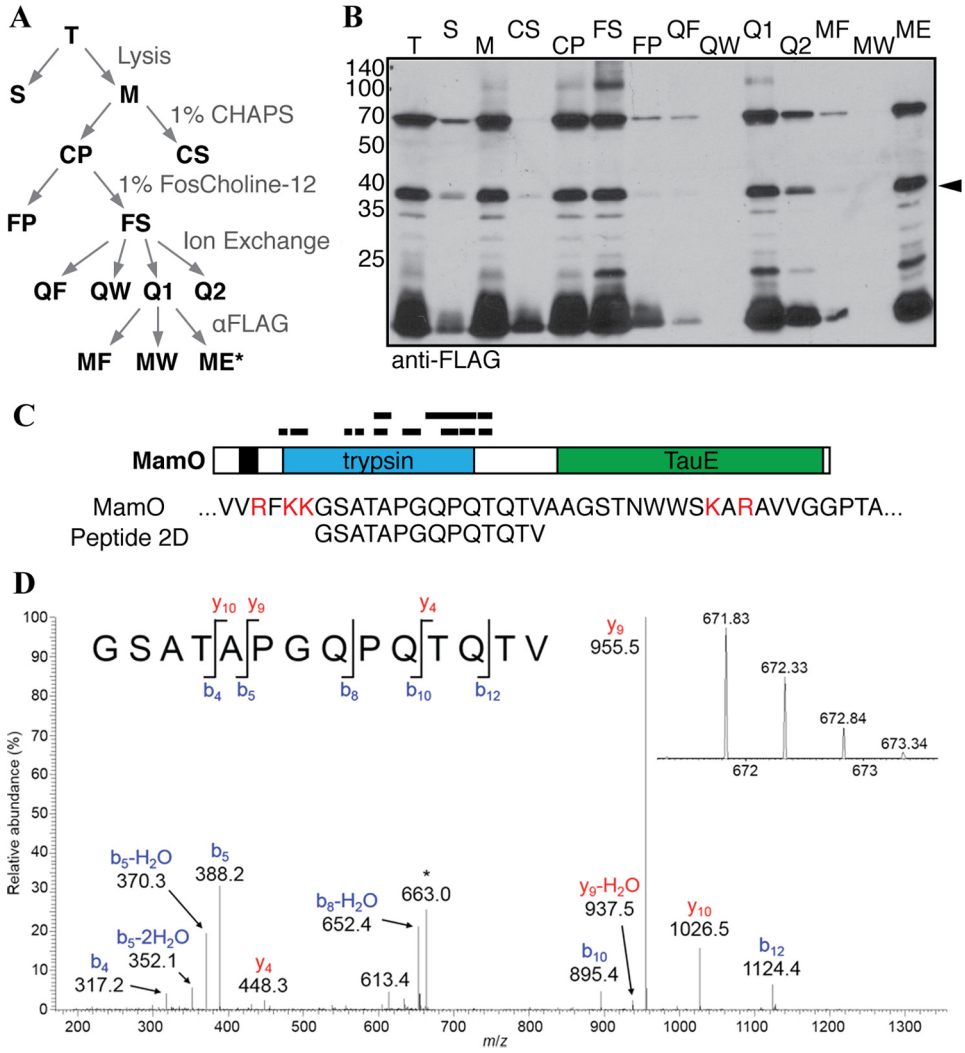

FIGURE 2. **Biochemical fractionation to enrich N-terminal MamO fragments.** *A*, schematic of the enrichment procedure. *B*, immunoblot of each fraction from *A*. The predicted protease domain fragment is marked with an *arrowhead*. *C*, peptides identified in a representative LC-MS/MS analysis. The *red letters* in the MamO sequence represent predicted tryptic cleavage sites. The coverage pattern is characteristic of analyses for three separate preparations. *D*, tandem mass spectrum from collision-induced dissociation of the $[M + 2H]^{2+}$ ion of the peptide, GSATAPGQPQTQTV, corresponding to amino acid residues 273–286 of MamO. *Inset*, detail for the isotopically resolved, unfragmented peptide precursor ion. The fragment ion at $m/z = 663$ (denoted by the *asterisk*) is due to a precursor ion that has undergone neutral loss of a molecule of water. This peptide was detected in each of three biological replicate experiments.

DDM by extensive washing before eluting with salt. This fraction was then used as the input for an α-FLAG affinity isolation to yield a final fraction enriched in N-terminal fragments of MamO (Fig. 2, *A* and *B*). The concentrated α-FLAG elution was separated on an SDS-PAGE gel and stained with colloidal Coomassie Blue, and the region around 37 kDa was excised. After performing in-gel trypsin digestion, peptides were extracted and concentrated for LC-MS/MS analysis. A number of peptides from the MamO sequence were consistently detected, and, as expected, they mapped almost exclusively to the protease domain of MamO (Fig. 2*C*). In all of the samples, the protein sequence coverage dropped off sharply in the linker between the protease and TauE domains (Fig. 2*C*). A peptide with the sequence GSATAPGQPQTQTV was routinely detected at the C-terminal edge of the peptide coverage (Fig. 2*D*). This peptide results from a predicted tryptic cleavage on the N terminus but has a non-tryptic C terminus, which suggests that it contains the C-terminal sequence of the mature MamO protease domain.

Direct Proteolysis of the MamO Cleavage Motif—We expressed and purified a form of MamE with the N-terminal membrane anchor removed to study proteolysis of the *in vivo* cleavage motif identified in MamO. The recombinant protein was targeted to the *E. coli* periplasm to allow for heme-loading of the *c*-type cytochrome motifs (Fig. 3). We designed a fluorogenic peptide containing the 8 residues of the putative cleavage motif identified in MamO (Fig. 2) flanked by an upstream fluorophore and a downstream fluorescence quencher. Normally, the peptide has low fluorescence due to interaction between the fluorophore and quencher. If the peptide is cleaved, the two fragments will separate, resulting in an increase in fluorescence. Upon the addition of the O1 peptide to purified MamE, there was a linear increase in fluorescence. Importantly, the $MamE^{S297A}$ protein did not alter the fluorescence, indicating the signal was due to serine protease activity from MamE (Fig. 4*A*). MamE hydrolyzed the O1 peptide with a k_{cat} of 0.64 ± 0.03 min^{-1} and a K_m of 6.1 ± 0.5 μM. Interestingly, the reaction was positively cooperative, displaying a Hill coefficient of 1.5 ± 0.1

(Fig. 4*B*) (18, 35). These values are similar to those reported for cleavage of peptide substrate by other trypsin-like proteases and confirm that MamE can efficiently cleave the motif identified in MamO (36). Combined with the *in vivo* analysis, these results confirm that MamO is a direct proteolytic target of MamE.

Reconstitution of MamE Autoproteolysis—Analysis of MamE processing in AMB-1 along with the extensive autoproteolysis during its expression in *E. coli* suggested that MamE is capable of autoproteolysis. However, purified MamE was relatively stable such that after 1 h of incubation at 30 °C, nearly all of the protein remained intact (Fig. 5*A*). The positive cooperativity observed for the steady-state kinetics of O1 peptide cleavage indicated that the catalytic activity of MamE could be stimulated by substrates. We reasoned that this mode of regulation might also lead to peptide-induced activation of autocleavage. Indeed, the MamO1 peptide stimulated degradation of full-length MamE in a dose-dependent manner, confirming that MamE activity can be stimulated by the presence of substrate (Fig. 5*A*).

Taking advantage of the distinct tags used to purify MamE, we examined the autocleavage fragmentation pattern by immunoblotting. Numerous truncated proteins were detected by blotting for the N-terminal His_6 tag, the smallest of which is a ~27-kDa fragment presumed to be the protease domain (Fig. 5*B*). In contrast, only the full-length protein was seen when blotting for the C-terminal Strep-tag (Fig. 5*C*). The pattern indicates that the reaction proceeds via sequential removal of small fragments from the C terminus. Furthermore, it matches the pattern seen by examining epitope-tagged alleles of MamE expressed *in vivo* and confirms the successful reconstitution MamE-dependent proteolysis *in vitro*.

Activation through the PDZ Domains—PDZ domains often regulate proteolytic activity by binding to extended peptide motifs (19). Phage display has been a productive approach for identifying peptide ligands that bind to PDZ domains (37–40). Each of the MamE PDZ domains was purified and used as bait in phage display selections. Both bait proteins showed phage enrichment for specific particles with a library displaying peptides on the N terminus of the coat protein, but no enrichment was observed in libraries displaying C-terminal fusions. This suggests that, unlike those associated with other HtrA proteases, the MamE PDZ domains do not display a preference for C-terminal peptides (30, 41). Interestingly, phage selections for both domains showed a strong preference for internal regions (Tables 3 and 4). However, a single clone dominated both pools, making the identification of consensus motifs hard to interpret.

Peptides corresponding to the sequence that dominated each selection were synthesized and labeled with a fluorescent dye. In addition, the C-terminal region of MamE containing only the PDZ domains (EP12) was purified and used to test for direct binding to the phage-derived ligands. Fluorescence anisotropy

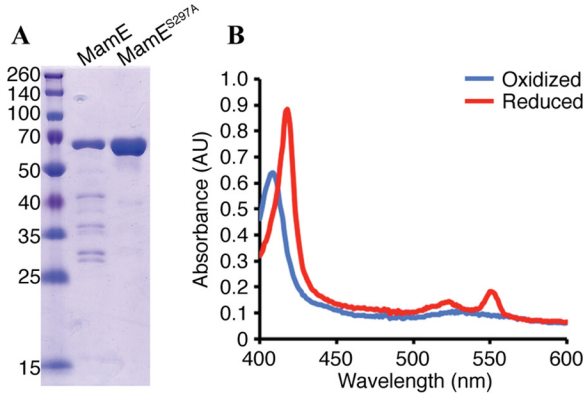

FIGURE 3. **Purification of MamE.** *A*, MamE and MamE^{S297A} (residues 108–728) were purified as a fusion to an N-terminal His_6 and C-terminal Strep-tag. *B*, absorbance spectrum of MamE^{S297A} in the oxidized (*blue*) and dithionite-reduced (*red*) forms.

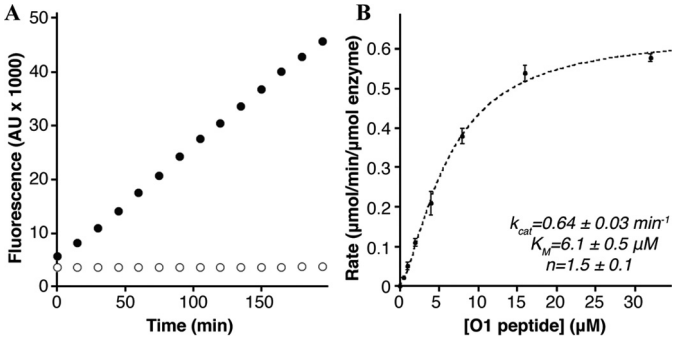

FIGURE 4. **Cleavage of the MamO1 fluorogenic substrate.** *A*, linear increase in fluorescence upon the addition of 20 μM MamO1 peptide to 200 nM MamE (*black circles*). No increase is seen with peptide addition to MamE^{S297A} (*white circles*). *B*, steady-state kinetics of O1 cleavage by MamE. The *dotted line* represents a fit to the Hill form of the Michaelis-Menten equation. *Error bars*, S.D. from three technical replicates. The plot is characteristic of the data seen in five biological replicates.

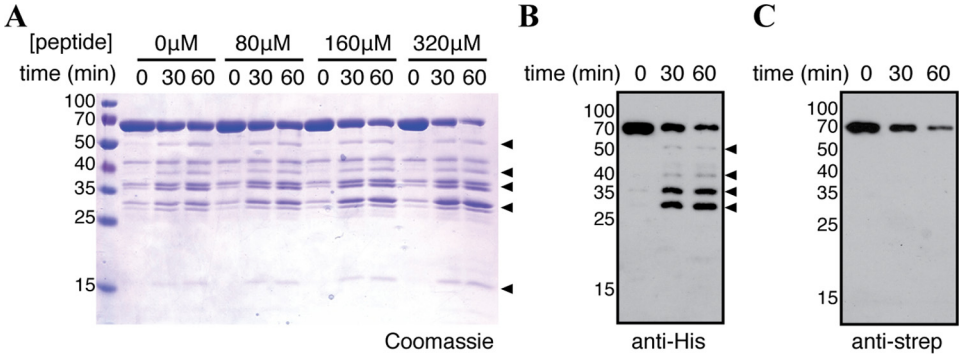

FIGURE 5. **Reconstitution of MamE autoprocessing.** *A*, MamO1 substrate induces autocleavage of MamE. *B* and *C*, processing patterns assessed by immunoblotting of a reaction containing 320 μM O1 for the indicated tag on MamE. The experiment is representative of three biological replicates. Throughout, proteolytic fragments increasing during the assay are marked with *arrowheads*.

TABLE 3

Peptide sequences from the phage display selections using MamE PDZ1

Each sequence was identified by isolating plaques from the enriched phage library and sequencing the gene for the major coat protein. The count represents the number of individual clones displaying the indicated peptide. The sequences are aligned based on the motif $\Psi XXX\Omega$, where Ψ is a hydrophilic residue and Ω is an aromatic residue. Bold type is used to mark the hydrophilic and aromatic residues around which the sequences were aligned.

Peptide Sequence	Count
- - W S Q E M **E** D W F **W** Q M P L S G - - - -	37
- - - - - - F **N** Y E Q **W** L Q A E Y L Q E H -	3
- - - - - D D **E** W W M **W** V E Q K L H E A T -	2
- - - - P E T **Q** Y W L **W** L M E L D S Q G - -	2
M L Y N F F E **Q** G W W **W** Y F S W - - - - - -	2
E D Q S K L D **Q** Y S K **W** M L M L - - - - - - -	1
- - I D T L V **E** H H W **W** G T V T T F - - - -	1
- - - - - - - P **E** F D E **W** F E Q R Y E E M E K	1
- - - - - - V F **D** Y W Q **W** V M E D T D G M I -	1
- - W E W P D **D** A W Q **F** L T R M S T - - - -	1
- - - - - - F **D** Y W E **Y** I S H A E Q P S D L	1

TABLE 4

Peptide sequences from the phage display selections using MamE PDZ2

Each sequence was identified by isolating plaques from the enriched phage library and sequencing the gene for the major coat protein. The count represents the number of individual clones displaying the indicated peptide. The sequences are aligned based on the motif $\Psi\Phi G\Phi\Phi\Phi$, where Ψ is a hydrophobic residue and Φ is a hydrophilic residue. Bold type is used to mark the glycine residue around which the sequences were aligned.

Peptide Sequence	Count
- - - - - - - - - M E D Y **G** I F M T S P E G P W A	22
- G Q I E P T W M W D M Y **G** F K L - - - - - - - -	2
S Y V P G E W Q G L E S M **G** I V M - - - - - - - -	2
- A Q E A D Y P A L Y Q L **G** F I P - - - - - - - -	1
- - E H W Q D Y S F E S L **G** I Y I - - - - - - - -	1
- E S P V E W D Y L E S F **G** L V I - - - - - - - -	1
- - - - - - E W S F Q D M **G** F M L S Y D Q M G - -	1
- - - - I A P D L W Y N W **G** I M W R D G - - - - -	1
- - I S Q E P L Y I E Q L **G** M M V F - - - - - - -	1
- - - - - - N E M D N L M **G** M I F M S P E - - -	1
- - - - - - N H A Y Q D F **G** F V V S E L Q E - - -	1
- - P F M P L E Y W Q F M **G** I V F T - - - - - - -	1
- - - - P G T F E D A T L **G** F T W F H D - - - - -	1
- Q N N Q D M M F Q P E L **G** I W F - - - - - - - -	1
- - - - R M P E S M R D M **G** F S I L M A - - - - -	1
- - - - - - Y H G V N E L **G** L M M M D Y I P - - -	1

experiments demonstrated that both phage-derived peptides bind to the C terminus of MamE (Fig. 6*A*). The PDZ1 peptide showed ~10-fold tighter binding than the PDZ2 peptide, but both affinities were comparable with those seen for other PDZ domains (40). The addition of either peptide to full-length MamE resulted in a dose-dependent activation of autoprocessing (Fig. 6*B*). Importantly, the activation threshold for the PDZ2 peptide was higher than for the PDZ1 peptide, mirroring the equilibrium binding data. Thus, ligand binding to either of the PDZ domains of MamE activates its autocleavage activity.

Misregulation of MamE Disrupts Biomineralization in Vivo—The switch-like activation of the MamE catalytic rate suggested that its activity is carefully modulated during biomineralization. Mutating residue 192 (chymotrypsin numbering) in the oxyanion hole to proline increases basal cleavage rates in the model HtrA protease DegS (18, 42). We introduced an allele with the analogous mutation of MamE (Q294P) into the *mamE* null strain (Fig. 7*A*). This strain displayed significantly less MamE and MamP, consistent with the expectation that the $MamE^{Q294P}$ variant is a more active protease. Additionally, the $mamE^{Q294P}$ allele partially circumvents the requirement for *mamO* in promoting MamE-dependent proteolysis. MamE and MamP were not processed when the $mamE^{WT}$ allele was introduced into a strain lacking *mamE* and *mamO*. However, when the $mamE^{Q294P}$ allele was introduced in the same background, proteolysis of MamE and MamP was restored, although processing of MamE did not reach wild-type levels (Fig. 7, *B* and *C*). The intermediate levels of MamE in the absence of MamO indicate that the $MamE^{Q294P}$ protein is not inherently unstable. These results show that $mamE^{Q294P}$ produces a misregulated protease, leading to increased processing of biomineralization factors *in vivo*.

We next examined the $mamE^{Q294P}$ allele for its ability to complement the biomineralization defects seen in the *mamE* null strain. Whereas the $mamE^{WT}$ allele completely restores the magnetic response, the $mamE^{Q294P}$ strain has a significantly lower response (Fig. 7*D*). Thus, both the inactive ($mamE^{PD}$) and misregulated forms ($mamE^{Q294P}$) of the protease disrupt biomineralization *in vivo*. The magnetic response of the $mamE^{Q294P}$ strain is higher than the negligible signal measured in the $mamE^{PD}$ strain, indicating that the biomineralization process is stalled at a different stage when the activity of MamE is unregulated. These results demonstrate that complete biomineralization of magnetosome crystals relies not only on the occurrence of MamE-dependent proteolysis but also careful regulation of the activity.

Discussion

Biochemical principles underlying the biomineralization of magnetite by magnetotactic bacteria represent a model for understanding how biological molecules manipulate inorganic compounds (43). Recent advances describing the genetic basis for this process have paved the way for mechanistic studies of the factors that promote mineral formation (6). Through these efforts, the HtrA protease MamE has emerged as a central biomineralization factor in the model organism *M. magneticum* AMB-1. In addition to promoting crystal nucleation within the magnetosome lumen, MamE regulates a transition from small superparamagnetic crystals to full-size paramagnetic particles. This crystal maturation phenotype was specifically linked to the putative protease activity of MamE, suggesting a model where its catalytic activity controls crystal maturation (13).

Here, we have studied the serine protease activity of MamE in detail. We have mapped the proteolytic patterns of three *in vivo* targets both at the domain level and, in one case, at the individual residue level. Using this information, we have reconstituted a number of aspects of MamE-dependent proteolysis with purified components. We show that MamE directly cleaves a motif from the linker between the MamO protease and TauE domains in a positively cooperative fashion. Furthermore, we show that purified MamE has low basal activity but that it can be activated in a number of ways, including the presence of substrate and peptide binding to either of its PDZ domains. This behavior is consistent with a switch-like mode of regulation in which the protease requires activation by environmental cues. These results also show for the first time that MamE is a

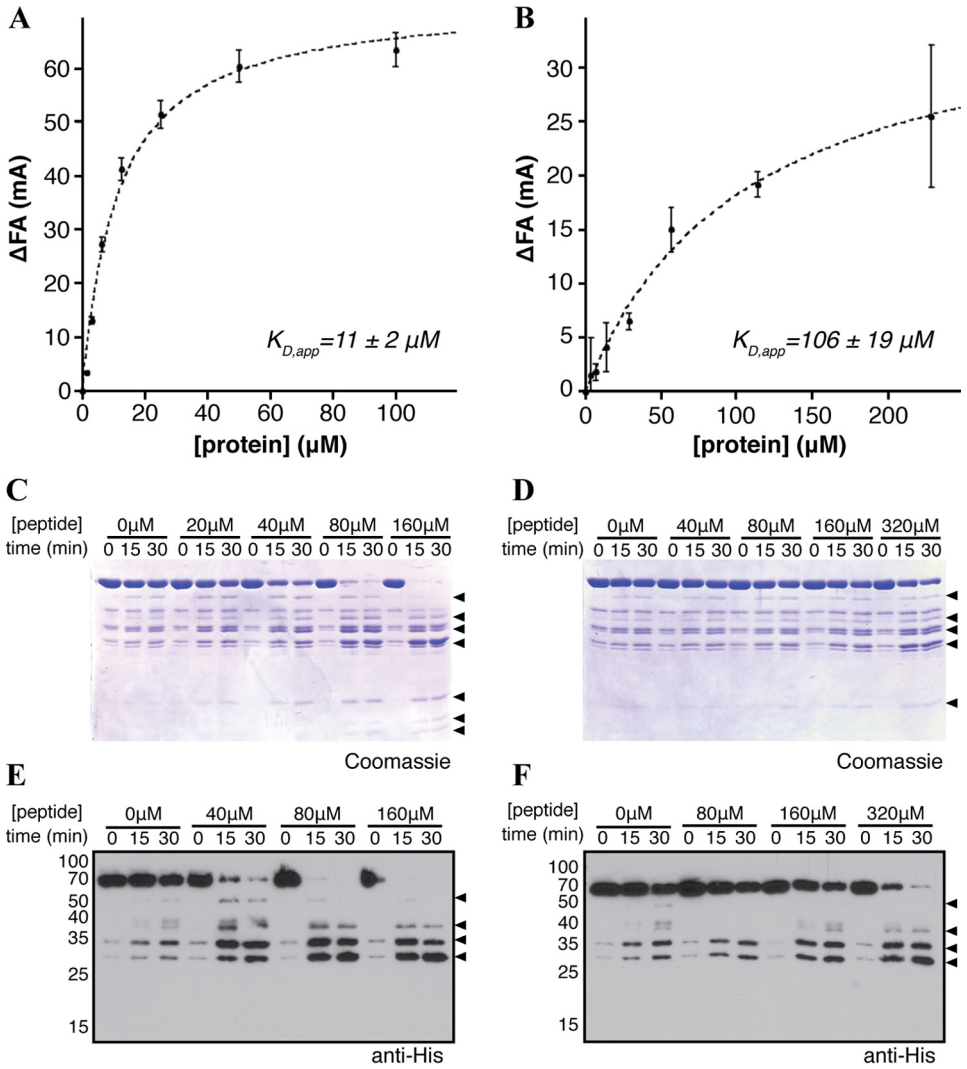

FIGURE 6. **Peptide binding to the PDZ domains activates MamE.** *A*, fluorescence anisotropy showing binding of the EPDZ1* peptide to the EP12 protein. *Error bars*, S.D. from three technical replicates. The *dotted line* represents a fit of the data to a single-site binding model. *B*, binding of the EPDZ2* peptide to the EP12 protein. *C*, activation of MamE autocleavage by the EPDZ1* peptide. *D*, activation of MamE autocleavage by the EPDZ2* peptide. Each experiment was repeated a minimum of three times. *E*, anti-His immunoblot of the reaction in *C*. *F*, anti-His immunoblot of the reaction in *D*. Throughout, proteolytic fragments increasing during the assay are marked with *arrowheads*. *Error bars*, S.D.

serine protease that is capable of directly degrading itself and other biomineralization factors.

The peptide-based substrate and ligands developed here shift MamE into the activated state *in vitro*, but the specific signals that activate the protein *in vivo* are not known. We previously showed that proteolysis of MamE, MamO, and MamP requires the presence of the C-terminal ion transporter domain of MamO, suggesting that manipulation of the solute environment in the magnetosome regulates the activity of MamE (24). However, the transport cargo(s) of MamO have not been identified, making the prediction of potential activating solutes difficult. In addition to its protease and PDZ domains, MamE contains a pair of *c*-type cytochrome motifs called magnetochrome domains that are commonly seen in magnetosome biomineralization proteins (Fig. 1*A*). The tandem magnetochrome region of MamE was previously purified and displayed a single midpoint redox potential of −32 mV, consistent with the proposed roles of similar biomineralization factors in controlling the redox status of iron (25, 26, 44). Although redox-mediated activation presents an attractive model for MamE regulation, we have not observed any redox dependence for the rate of autoproteolysis or steady-state cleavage of the MamO1 peptide.

Despite the uncertainty about the specific events that trigger its activation, the switch-like modulation of MamE activity *in vitro* suggested that allosteric regulation of its protease activity was required for proper crystal maturation. We developed an allele of MamE with a mutation reported to stabilize active forms of other HtrA proteases and showed that this allele no longer required *mamO* to promote proteolysis *in vivo*. Like the catalytically inactive form, this misregulated form of MamE had defects in crystal maturation (18). These results confirm that both the active and inactive states are important during the process of magnetosome formation. Similar experiments with DegP in *E. coli* indicated that the proper balance between active and inactive forms is required for fitness during heat stress (45). Our results show that, in addition to maintaining fitness during stress, this mode of regulation can be used to control a developmental process.

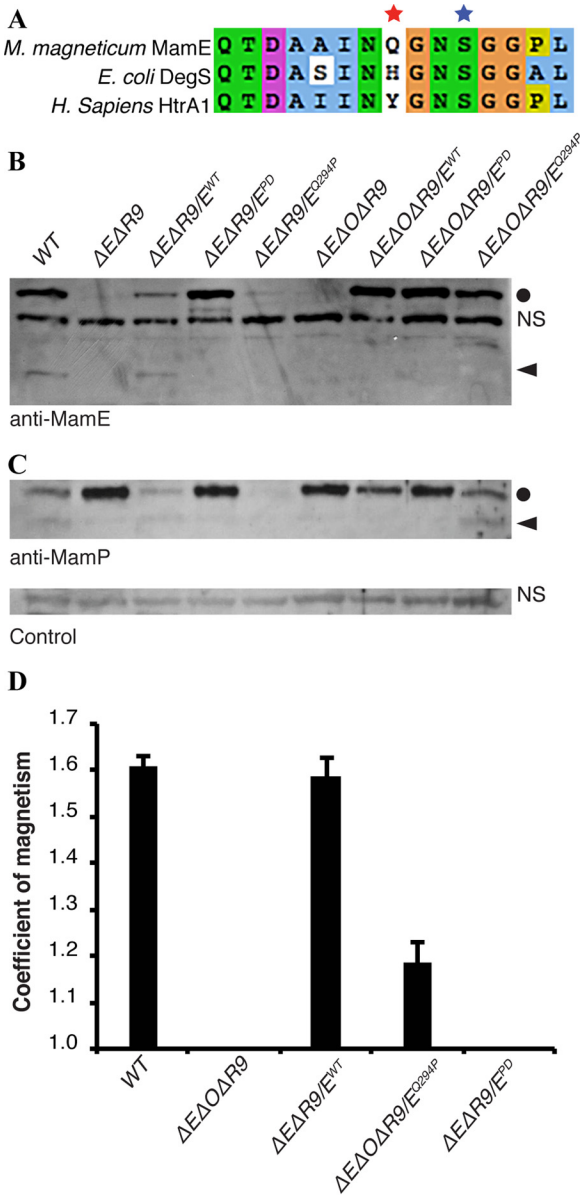

FIGURE 7. **A constitutively active form of MamE disrupts biomineralization.** *A*, alignment of HtrA proteases. The *red star* marks position 192 in the oxyanion hole (residue 198 in DegS), and the *blue star* marks the catalytic serine nucleophile. *B* and *C*, immunoblot analysis of AMB-1 lysates probed for MamE (*B*) and MamP (*C*). *Circles* mark full-length proteins, and *arrowheads* mark proteolytic fragments. *NS*, nonspecific bands reacting with each antibody preparation. *D*, magnetic response of AMB-1 cultures with the indicated genetic background. Biological replicates represent independent cultures of each strain, and each measurement represents the average and S.D. from three independent experiments. *Error bars*, S.D.

Nearly all studied members of the HtrA family behave as trimers or multiples thereof (15–17, 22, 46, 47). In other systems with two PDZ domains, the first PDZ seems to regulate protease activity directly, whereas the second is thought to mediate rearrangements of core trimers into higher order oligomers (20, 22, 23). Peptide binding to either the first or the second PDZ domain of MamE can activate proteolysis, although the activation through PDZ2 is much weaker. Furthermore, the protein behaves as a monomer, as indicated by gel filtration. Transitions between a monomer and higher order assemblies are rare in the HtrA family, but the positive cooperativity observed for MamE suggests that the active form is indeed a larger assembly (48). The protein production method described here should enable future structural studies aimed at understanding the potential for novel assembly behavior as well as an unusual regulatory role for the second PDZ domain.

Taken together, our results support the checkpoint model for MamE-dependent proteolysis in regulating the maturation of magnetite crystals. However, the detailed mechanism by which that activity promotes crystal growth remains unclear. One possible mechanism could be by controlling the size of the surrounding membrane. A recent study demonstrated a link between the growth of magnetosome membrane compartments and growth of the magnetite crystals within. This finding led to the proposal that there is a checkpoint regulating a second stage of membrane growth after the onset of biomineralization (49). In addition to biomineralization defects, proteins normally targeted to the magnetosome membrane are dispersed throughout the cytoplasmic membrane in a *mamE* deletion, suggesting an additional defect in magnetosome membrane organization (6, 13). Magnetosome membrane sizes have not been quantified in this strain. It is tempting to speculate that proteolysis controls a switch that links membrane growth to crystal growth. In this scenario, crystal nucleation in the E^{PD} cells would not lead to membrane growth, whereas the E^{QP} cells would initiate membrane growth before crystals had grown sufficiently, leading to stunted particles in both cases.

Author Contributions—D. M. H. coordinated the study, performed majority of experiments, and wrote the paper. A. K. coordinated the study, advised on experiments, and edited paper. P. J. B. designed and performed experiments on the constitutive MamE mutant. A. T. I. advised on and performed mass spectrometry experiments. E. H. L. purified MamE PDZ domains. J. T. and S. S. S. coordinated and performed phage display experiments to identify peptides that bound to MamE PDZ domains. All authors reviewed the results and approved the final version of the manuscript.

Acknowledgments—The QB3/Chemistry Mass Spectrometry Facility at the University of California (Berkeley, CA) is supported by National Institutes of Health Grant 1S10OD020062-01.

References

1. Blakemore, R. (1975) Magnetotactic bacteria. *Science* **190,** 377–379
2. Balkwill, D. L., Maratea, D., and Blakemore, R. P. (1980) Ultrastructure of a magnetotactic spirillum. *J. Bacteriol.* **141,** 1399–1408
3. Wolff, A., Frese, K., Wiβbrock, M., Eckstädt, K., Ennen, I., Hetaba, W., Löffler, S., Regtmeier, A., Thomas, P., Sewald, N., Schattschneider, P., and Hütten, A. (2012) Influence of the synthetic polypeptide c25-mms6 on cobalt ferrite nanoparticle formation. *J. Nanopart. Res.* **14,** 1161
4. Kashyap, S., Woehl, T. J., Liu, X., Mallapragada, S. K., and Prozorov, T. (2014) Nucleation of iron oxide nanoparticles mediated by Mms6 protein *in situ*. *ACS Nano* **8,** 9097–9106
5. Rawlings, A. E., Bramble, J. P., Walker, R., Bain, J., Galloway, J. M., and Staniland, S. S. (2014) Self-assembled MmsF proteinosomes control magnetite nanoparticle formation *in vitro*. *Proc. Natl. Acad. Sci. U.S.A.* **111,** 16094–16099
6. Murat, D., Quinlan, A., Vali, H., and Komeili, A. (2010) Comprehensive genetic dissection of the magnetosome gene island reveals the step-wise assembly of a prokaryotic organelle. *Proc. Natl. Acad. Sci. U.S.A.* **107,** 5593–5598
7. Lohsse, A., Ullrich, S., Katzmann, E., Borg, S., Wanner, G., Richter, M.,

Voigt, B., Schweder, T., and Schüler, D. (2011) Functional analysis of the magnetosome island in *Magnetospirillum gryphiswaldense*: the mamAB operon is sufficient for magnetite biomineralization. *PLoS One* **6,** e25561
8. Lohsse, A., Borg, S., Raschdorf, O., Kolinko, I., Tompa, E., Pósfai, M., Faivre, D., Baumgartner, J., and Schüler, D. (2014) Genetic dissection of the mamAB and mms6 operons reveals a gene set essential for magnetosome biogenesis in *Magnetospirillum gryphiswaldense*. *J. Bacteriol.* **196,** 2658–2669
9. Kolinko, I., Lohsse, A., Borg, S., Raschdorf, O., Jogler, C., Tu, Q., Pósfai, M., Tompa, E., Plitzko, J. M., Brachmann, A., Wanner, G., Müller, R., Zhang, Y., and Schüler, D. (2014) Biosynthesis of magnetic nanostructures in a foreign organism by transfer of bacterial magnetosome gene clusters. *Nat. Nanotechnol.* **9,** 193–197
10. Rahn-Lee, L., Byrne, M. E., Zhang, M., Le Sage, D., Glenn, D. R., Milbourne, T., Walsworth, R. L., Vali, H., and Komeili, A. (2015) A genetic strategy for probing the functional diversity of magnetosome formation. *PLoS Genet.* **11,** e1004811
11. Yang, W., Li, R., Peng, T., Zhang, Y., Jiang, W., Li, Y., and Li, J. (2010) *mamO* and *mamE* genes are essential for magnetosome crystal biomineralization in *Magnetospirillum gryphiswaldense* MSR-1. *Res. Microbiol.* **161,** 701–705
12. Komeili, A., Li, Z., Newman, D. K., and Jensen, G. J. (2006) Magnetosomes are cell membrane invaginations organized by the actin-like protein MamK. *Science* **311,** 242–245
13. Quinlan, A., Murat, D., Vali, H., and Komeili, A. (2011) The HtrA/DegP family protease MamE is a bifunctional protein with roles in magnetosome protein localization and magnetite biomineralization. *Mol. Microbiol.* **80,** 1075–1087
14. Clausen, T., Kaiser, M., Huber, R., and Ehrmann, M. (2011) HtrA proteases: regulated proteolysis in protein quality control. *Nat. Rev. Mol. Cell Biol.* **12,** 152–162
15. Krojer, T., Garrido-Franco, M., Huber, R., Ehrmann, M., and Clausen, T. (2002) Crystal structure of DegP (HtrA) reveals a new protease-chaperone machine. *Nature* **416,** 455–459
16. Wilken, C., Kitzing, K., Kurzbauer, R., Ehrmann, M., and Clausen, T. (2004) Crystal structure of the DegS stress sensor: how a PDZ domain recognizes misfolded protein and activates a protease. *Cell* **117,** 483–494
17. Li, W., Srinivasula, S. M., Chai, J., Li, P., Wu, J.-W., Zhang, Z., Alnemri, E. S., and Shi, Y. (2002) Structural insights into the pro-apoptotic function of mitochondrial serine protease HtrA2/Omi. *Nat. Struct. Biol.* **9,** 436–441
18. Sohn, J., Grant, R. A., and Sauer, R. T. (2010) Allostery is an intrinsic property of the protease domain of DegS: implications for enzyme function and evolution. *J. Biol. Chem.* **285,** 34039–34047
19. Krojer, T., Sawa, J., Huber, R., and Clausen, T. (2010) HtrA proteases have a conserved activation mechanism that can be triggered by distinct molecular cues. *Nat. Struct. Mol. Biol.* **17,** 844–852
20. Kim, S., Grant, R. A., and Sauer, R. T. (2011) Covalent linkage of distinct substrate degrons controls assembly and disassembly of DegP proteolytic cages. *Cell* **145,** 67–78
21. Sohn, J., Grant, R. A., and Sauer, R. T. (2007) Allosteric activation of DegS, a stress sensor PDZ protease. *Cell* **131,** 572–583
22. Wrase, R., Scott, H., Hilgenfeld, R., and Hansen, G. (2011) The *Legionella* HtrA homologue DegQ is a self-compartmentizing protease that forms large 12-meric assemblies. *Proc. Natl. Acad. Sci. U.S.A.* **108,** 10490–10495
23. Krojer, T., Sawa, J., Schäfer, E., Saibil, H. R., Ehrmann, M., and Clausen, T. (2008) Structural basis for the regulated protease and chaperone function of DegP. *Nature* **453,** 885–890
24. Hershey, D. M., Ren, X., Melnyk, R. A., Browne, P. J., Ozyamak, E., Jones, S. R., Chang, M. C. Y., Hurley, J. H., and Komeili, A. (2016) MamO is a repurposed serine protease that promotes magnetite biomineralization through direct transition metal binding in magnetotactic bacteria. *PLoS Biol.* **14,** e1002402
25. Siponen, M. I., Legrand, P., Widdrat, M., Jones, S. R., Zhang, W.-J., Chang, M. C. Y., Faivre, D., Arnoux, P., and Pignol, D. (2013) Structural insight into magnetochrome-mediated magnetite biomineralization. *Nature* **502,** 681–684
26. Jones, S. R., Wilson, T. D., Brown, M. E., Rahn-Lee, L., Yu, Y., Fredriksen, L. L., Ozyamak, E., Komeili, A., and Chang, M. C. Y. (2015) Genetic and biochemical investigations of the role of MamP in redox control of iron biomineralization in *Magnetospirillum magneticum*. *Proc. Natl. Acad. Sci. U.S.A.* **112,** 3904–3909
27. Roepstroff, P., and Fohlman, J. (1984) Proposal for a common nomenclature for sequence ions in mass spectra of peptides. *Biomed. Mass Spectrom.* **11,** 601
28. Londer, Y. Y., Pokkuluri, P. R., Orshonsky, V., Orshonsky, L., and Schiffer, M. (2006) Heterologous expression of dodecaheme "nanowire" cytochromes c from *Geobacter sulfurreducens*. *Protein Expr. Purif.* **47,** 241–248
29. Arslan, E., Schulz, H., Zufferey, R., Künzler, P., and Thöny-Meyer, L. (1998) Overproduction of the *Bradyrhizobium japonicum* c-type cytochrome subunits of the cbb3 oxidase in *Escherichia coli*. *Biochem. Biophys. Res. Commun.* **251,** 744–747
30. Laura, R. P., Witt, A. S., Held, H. A., Gerstner, R., Deshayes, K., Koehler, M. F. T., Kosik, K. S., Sidhu, S. S., and Lasky, L. A. (2002) The Erbin PDZ domain binds with high affinity and specificity to the carboxyl termini of δ-catenin and ARVCF. *J. Biol. Chem.* **277,** 12906–12914
31. Held, H. A., and Sidhu, S. S. (2004) Comprehensive mutational analysis of the M13 major coat protein: improved scaffolds for C-terminal phage display. *J. Mol. Biol.* **340,** 587–597
32. Arita, Y., Allen, S., Chen, G., Zhang, W., Wang, Y., Owen, A. J., Dentinger, P., and Sidhu, S. S. (2016) Rapid isolation of peptidic inhibitors of the solute carrier family transporters OATP1B1 and OATP1B3 by cell-based phage display selections. *Biochem. Biophys. Res. Commun.* **473,** 370–376
33. Tonikian, R., Zhang, Y., Boone, C., and Sidhu, S. S. (2007) Identifying specificity profiles for peptide recognition modules from phage-displayed peptide libraries. *Nat. Protoc.* **2,** 1368–1386
34. Tonikian, R., Zhang, Y., Sazinsky, S. L., Currell, B., Yeh, J.-H., Reva, B., Held, H. A., Appleton, B. A., Evangelista, M., Wu, Y., Xin, X., Chan, A. C., Seshagiri, S., Lasky, L. A., Sander, C., Boone, C., Bader, G. D., and Sidhu, S. S. (2008) A specificity map for the PDZ domain family. *PLoS Biol.* **6,** e239
35. Mauldin, R. V., and Sauer, R. T. (2013) Allosteric regulation of DegS protease subunits through a shared energy landscape. *Nat. Chem. Biol.* **9,** 90–96
36. Small, J. L., O'Donoghue, A. J., Boritsch, E. C., Tsodikov, O. V., Knudsen, G. M., Vandal, O., Craik, C. S., and Ehrt, S. (2013) Substrate specificity of MarP, a periplasmic protease required for resistance to acid and oxidative stress in *Mycobacterium tuberculosis*. *J. Biol. Chem.* **288,** 12489–12499
37. Fuh, G., Pisabarro, M. T., Li, Y., Quan, C., Lasky, L. A., and Sidhu, S. S. (2000) Analysis of PDZ domain-ligand interactions using carboxyl-terminal phage display. *J. Biol. Chem.* **275,** 21486–21491
38. Zhang, Y., Appleton, B. A., Wu, P., Wiesmann, C., and Sidhu, S. S. (2007) Structural and functional analysis of the ligand specificity of the HtrA2/Omi PDZ domain. *Protein Sci.* **16,** 1738–1750
39. Runyon, S. T., Zhang, Y., Appleton, B. A., Sazinsky, S. L., Wu, P., Pan, B., Wiesmann, C., Skelton, N. J., and Sidhu, S. S. (2007) Structural and functional analysis of the PDZ domains of human HtrA1 and HtrA3. *Protein Sci.* **16,** 2454–2471
40. Ivarsson, Y., Arnold, R., McLaughlin, M., Nim, S., Joshi, R., Ray, D., Liu, B., Teyra, J., Pawson, T., Moffat, J., Li, S. S. C., Sidhu, S. S., and Kim, P. M. (2014) Large-scale interaction profiling of PDZ domains through proteomic peptide-phage display using human and viral phage peptidomes. *Proc. Natl. Acad. Sci. U.S.A.* **111,** 2542–2547
41. Lee, H.-J., and Zheng, J. J. (2010) PDZ domains and their binding partners: structure, specificity, and modification. *Cell Commun. Signal.* **8,** 8–18
42. Perona, J. J., and Craik, C. S. (1997) Evolutionary divergence of substrate specificity within the chymotrypsin-like serine protease fold. *J. Biol. Chem.* **272,** 29987–29990
43. Komeili, A. (2012) Molecular mechanisms of compartmentalization and biomineralization in magnetotactic bacteria. *FEMS Microbiol. Rev.* **36,** 232–255
44. Siponen, M. I., Adryanczyk, G., Ginet, N., Arnoux, P., and Pignol, D. (2012) Magnetochrome: a c-type cytochrome domain specific to magnetotatic bacteria. *Biochem. Soc. Trans.* **40,** 1319–1323
45. Kim, S., and Sauer, R. T. (2014) Distinct regulatory mechanisms balance

DegP proteolysis to maintain cellular fitness during heat stress. *Genes Dev.* **28,** 902–911

46. Mohamedmohaideen, N. N., Palaninathan, S. K., Morin, P. M., Williams, B. J., Braunstein, M., Tichy, S. E., Locker, J., Russell, D. H., Jacobs, W. R., Jr., and Sacchettini, J. C. (2008) Structure and function of the virulence-associated high-temperature requirement A of *Mycobacterium tuberculosis*. *Biochemistry* **47,** 6092–6102
47. Truebestein, L., Tennstaedt, A., Mönig, T., Krojer, T., Canellas, F., Kaiser, M., Clausen, T., and Ehrmann, M. (2011) Substrate-induced remodeling of the active site regulates human HtrA1 activity. *Nat. Struct. Mol. Biol.* **18,** 386–388
48. Kley, J., Schmidt, B., Boyanov, B., Stolt-Bergner, P. C., Kirk, R., Ehrmann, M., Knopf, R. R., Naveh, L., Adam, Z., and Clausen, T. (2011) Structural adaptation of the plant protease Deg1 to repair photosystem II during light exposure. *Nat. Struct. Mol. Biol.* **18,** 728–731
49. Cornejo, E., Subramanian, P., Li, Z., Jensen, G. J., and Komeili, A. (2016) Dynamic remodeling of the magnetosome membrane is triggered by the initiation of biomineralization. *mBio* **7,** e01898–15